RSC Advances

ROYAL SOCIETY OF CHEMISTRY

www.rsc.org/advances

Nanosized Surface Films on Brass Alloys by XPS and XAES

Federica Cocco[1)], Bernhard Elsener[1) 2)], Marzia Fantauzzi[1)], Davide Atzei[1)], Antonella Rossi[1)]*

1) Dipartimento di Scienze Chimiche e Geologiche, Università degli Studi di Cagliari, Campus di Monserrato S.S. 554 – Italy and INSTM, UdR Cagliari – Italy
2) ETH Zurich, Institute for Building Materials, ETH Hönggerberg, CH-8093 Zurich

* Corresponding author

Abstract

Chemical state identification and quantification based on photoelectron spectra is challenging in the case of copper and zinc and their alloys. In this work an analytical strategy for simultaneous chemical state identification and quantification of copper and zinc chemical state in complex layered systems is presented. This approach is based on the curve fitting of the multicomponent X-ray excited Auger spectra: $CuL_3M_{4,5}M_{4,5}$ and $ZnL_3M_{4,5}M_{4,5}$, that clearly distinguish metallic and oxide components and result in separated $I_{LMM,met}$ and $I_{LMM,ox}$ peak areas. On reference copper and zinc compounds, showing only a single chemical state, the intensity ratio R between photoelectron I_{2p} and Auger intensity I_{LMM} was determined. R_{met} was obtained using pure metals and a sputtered brass alloy Cu37Zn. R_{ox} was calculated using the pure oxides. Based on these experimental intensity ratios R a quantification factor $k = R_{ox}/R_{met}$ is calculated for both copper and zinc. This quantification factor k is independent of the instrument employed for the analysis as here proved by using different spectrometers. The factor k is then used to transfer the experimental Auger intensity ratio ($I_{LMM,met}$ / $I_{LMM,ox}$) into the $I_{2p,met}$ / $I_{2p,ox}$ intensity ratio which is required for the quantitative analysis by XPS. The potential of this approach based on XPS and XAES for the patina studies on copper alloys, relevant in various field including corrosion and cultural heritage, is presented for Cu37Zn model brass alloy after different surface pre-treatments. This approach has proven to be successful.

Keywords:
Copper-Zinc alloys, Brass, X-ray photoelectron spectroscopy, XAES, Chemical state, Wagner plot, Quantitative analysis.

1. Introduction

The identification of the chemical environment for most elements can be routinely based on the measurement of the binding energy (BE) of the x-ray photoelectron signals and on the comparison with the values provided in databases such as NIST Database [1], PHI Handbook [2] or in books data compilations[3] It is however well known that this approach is very difficult for copper and zinc compounds due to the fact that the chemical shift between the elemental state and the oxidized one is very small. Recently [4], BE data from the NIST database has been revised. Metallic copper Cu (0) is reported at a BE of 932.61 eV (std. dev. = 0.21 eV) while the same signal in the case of copper oxide Cu_2O, is at a BE of 932.43 eV (std. dev. = 0.24 eV). These two chemical states of copper have thus statistically the same BE and cannot be differentiated setting the experimental conditions commonly used by laboratory spectrometers. In the case of zinc the situation is similar: metallic zinc Zn(0) has a BE of 1021.65 eV (std. dev. = 0.01 eV) whereas in zinc oxide ZnO, Zn(II) has a BE of 1021.00 eV (std. dev. = 0.04 eV). Also in this case a univocal identification of the zinc chemical state is challenging. In more complex systems such as copper/zinc alloys with nanometre-thick oxide over-layers the peaks will largely overlap and make identification of the chemical state and quantification of the species in the various layers even more difficult. A close inspection of the shape of the x-ray induced Auger signals $CuL_3M_{4,5}M_{4,5}$ and $ZnL_3M_{4,5}M_{4,5}$ together with the calculation of the Auger parameter greatly improve the assignment of the chemical state as it has been shown in several works for both copper [5 – 8, 11] and zinc compounds [9 – 11]. Despite the fact that Auger signals are sensitive to changes in the chemical state, the quantification when both chemical states of copper and zinc are simultaneously present is made difficult by the presence of a large number of signals. In few studies the quantification based on the x-ray excited Auger signals have been undertaken: a first attempt of curve fitting of the x-ray induced Auger signals of Cu and Cu_2O was reported in 1988 [12]. The same group [13] reported CuL_3MM spectra of Cu, Cu_2O, $Cu(OH)_2$ and CuO with an empirically-based curve fitting of the Auger signals. The ratio between Cu2p and Cu L_3MM intensity was discussed and a cross section σ_{L_3MM} for the Auger signals identical for oxidized and metallic compounds was experimentally deduced. A later work [14] on copper-zinc alloys in borate buffer solutions exploited the

same approach to fit $CuL_3M_{4,5}M_{4,5}$ and $ZnL_3M_{4,5}M_{4,5}$ Auger spectra of Cu, Zn, Cu_2O and ZnO. The assumption of a constant σ_{L_3MM} was maintained and no complex Auger spectra with simultaneous presence of metal and oxide components (e.g. Cu_2O on Cu, ZnO on Zn) were reported so that also the quantitative results are provided for a simple system.

In this work an analytical strategy for simultaneous chemical state identification and full quantification of copper and zinc, when occurring in complex nanostructured systems such as brass alloys with thin oxide - hydroxide surface films or patinas, is presented. The approach relies on the curve-fitting based on the theoretical description of the multicomponent XAES signals $CuL_3M_{4,5}M_{4,5}$ and $ZnL_3M_{4,5}M_{4,5}$ aiming to carefully determine the intensity (percentage) of the metallic and oxidized copper and/or zinc components. This percentage, after the correction for the intensity ratio 2p/LMM calculated on pure zinc and copper metal and zinc and copper oxides, is then used for converting them to the areas of $Cu2p_{3/2}$ or Zn $2p_{3/2}$ signals used for the subsequent quantification. The approach has been tested on Cu37Zn model brass alloy after different surface pre-treatments and has proven to be successful.

This approach has been developed in the framework of a wide research project[15] aiming to control the conditions that might cause damage on historical brass musical instruments and represents the starting point to relate non – destructive electrochemical tests to their surface chemistry.

2. Material and methods

2.1. Material and surface preparation

Pure copper and zinc metals (foils, purity > 99.9%, purchased from Goodfellow Cambridge Ltd, UK) and copper and zinc oxides (CuO 99.999%, $Cu_2O \geq 99{,}99\%$ anhydrous and $ZnO \geq 99.0\%$) supplied by Sigma Aldrich, Sant Louis, USA) were analysed in this work as reference materials.

A model brass alloy Cu37Zn (Goodfellow Cambridge Ltd, UK) in the "as received" state, after mechanical polishing and after Ar^+ sputtering was used for testing the analytical approach. Its certified composition is reported to be 63% Cu, 37% Zn.

The mechanical polishing procedure is required for a well-defined starting point of the investigated surfaces. The sample was first delicately ground with silica paper (grit sizes of 2400 and 4000) and then polished using a DP Dur cloth and diamond paste with grain diameters of 3, 1 and ¼ µm (Struers, Ballerup– DK). Ethanol (p.a.), supplied by J.T.Baker® Chemicals (Avantor Performance Materials, Inc. Global Headquarters, USA) was used for cooling, lubricating and for cleaning the samples in ultra-sonic bath for five minutes. The surface was dried under an argon stream and immediately introduced in the spectrometer.

Pure copper, zinc and brass samples were also investigated after ion sputtering using an acceleration voltage of 3 kV and an ion current of 1 µA for a maximum of 300 s. These conditions were chosen in order to remove the contamination and the oxidized layers until the complete disappearance of C1s and O1s signals.

2.2. X-ray photoelectron spectroscopy and data processing

Instruments: XP-spectra were acquired using a Theta Probe instrument (Thermo Fisher Scientific, East Grinstead, UK) and a PHI Quantera^{SXM} spectrometer (ULVAC-PHI, Chanhassen, MN, USA). Samples were mounted on a standard sample holder for XPS measurements with copper clips.

Theta Probe: The analyses were carried out with a monochromatic AlKα source (energy = 1486.6 eV)

selecting a spot size of 300 μm. The beam was operated at 4.7 mA and 15 kV (70 W). The instrument is equipped with an argon ion gun. For sputtering experiments an acceleration voltage of 3 kV and an ion current of 1 μA were used in this work. The residual pressure in the main chamber during the acquisition was lower than 10^{-7} Pa. The average emission angle is 53° while the angle between the source and the analyser axis 67.38°.

PHI Quantera: the instrument is equipped with a focused and scanned AlKα (energy = 1486.6 eV) source. The beam diameter was 100 μm and it was operated at 4 mA and 15 kV (60 W). The instrument is equipped with an argon ion gun. Argon ion sputtering was performed on 3x3 mm area, applying an acceleration voltage of 3 kV and measuring an ion current of 15 mA. The emission angle is of 45° and the angle between the source and the analyser axis is 45°.

Data acquisition:

Theta Probe: Survey and high-resolution spectra were acquired in fixed analyser transmission mode (FAT) setting the pass energy equal to 200 eV and to 100 eV respectively selecting the standard lens mode. Step-size was 1 eV and 0.05 eV, respectively. The full-width at half-maximum (FWHM) of the silver $Ag3d_{5/2}$ signal for the high-resolution spectra was 0.84 eV. The spectrometer was calibrated according to ISO 15472:2001 with an accuracy of ± 0.1 eV.

PHI Quantera: Survey and high-resolution spectra were acquired in fixed analyser transmission mode (FAT) setting the pass energy equal to 280 eV and to 69 eV respectively. Step-size was 1 eV and 0.125 eV, respectively. The FWHM of the silver $Ag3d_{5/2}$ signal for the high-resolution spectra was 0.79 eV. The spectrometer was calibrated according to ISO 15472:2010 [Surface Chemical Analysis – X-ray Photoelectron Spectrometers – Calibration of energy scales]. The accuracy was found to be equal to ± 0.1 eV

When necessary, the BE values were referenced to the aliphatic carbon at 285.0 eV. Data were acquired under computer control (Advantage v. 3.45). Three different regions were analysed on each sample. BE values and atomic percentages are reported in this work as mean values on three points with their corresponding standard deviations.

Data processing: The high-resolution spectra were processed using CASAXPS software [16]. The background was subtracted according to the Shirley-Sherwood background subtraction routine [17] prior to the curve fitting. This background subtraction routine was selected since this model is the most popular in practical surface analysis. It is worth to emphasise that Tougaard's background was also applied to the sputtered cleaned alloy and its composition was in excellent agreement with the one obtained by Shirley's background subtraction. Gaussian and Lorentzian (GL) product functions were used for curve fitting. Quantitative analysis of "as received" and sputter-cleaned brass surfaces were performed on the basis of the integrated intensity using the first-principle model [3] assuming the sample homogeneity. The atomic concentrations of the etched samples were calculated using the equation:

$$x_j = \frac{\frac{I_{ij}}{S_{ij}}}{\sum_j \frac{I_{ij}}{S_{ij}}} \qquad \text{eq. (1)}$$

where I is the measured peak area in Cps*eV and S is the sensitivity factor of the peak i of the element j. The sensitivity factors were calculated using Scofield's photoionization cross-section [18] corrected for the asymmetry factors [19], the analyser transmission function $T(E_i)$ of the instrument [20] and the inelastic mean free paths (IMFP). The IMFP was calculated using the equation proposed by Tanuma et al. [21]. The accuracy of the calculated atomic concentrations is estimated to be ± 10%.

Quantitative analysis of the brass surfaces covered with a thin oxide film (e.g. after mechanical polishing) was performed according to the three-layer model [22], the thickness and composition of the oxide layer and the composition of the metal phase beneath the film could be calculated from a single XPS/XAES measurement.

3. Results

In the first part of this section the XPS results of reference materials are presented. In the second part, the XPS results of the Cu37Zn brass model alloy are shown.

3.1. Reference materials

3.1.1. Copper and zinc metals

In order to obtain the curve-fitting parameters of the pure metals, copper and zinc foils were analysed as reference materials by XPS acquiring the high-resolution spectra $Cu2p_{3/2}$ and $CuL_3M_{4,5}M_{4,5}$ for copper and $Zn2p_{3/2}$ and $ZnL_3M_{4,5}M_{4,5}$ for zinc. The analysis was carried out after sputtering with Ar^+ ions to remove the contamination layer and the oxide film present at the surfaces. The survey spectra (not shown) of both metals showed only signals from Cu and Zn. No oxygen and carbon signals were revealed.

Copper: The $Cu2p_{3/2}$ region is shown in Figure SI1a (Electronic supplementary material) and the data are listed in Table SI1. The maximum of the signal was found at 932.5 (0.1) eV in agreement with the literature [8, 11-14]. The $CuL_3M_{45}M_{45}$ XAES signal (Figure SI 1b) shows a complex fine structure. Peaks related to the ^1S, ^3P, ^1D, ^3F and ^1G final states could be identified in agreement with literature [23 – 25]. The most intense peak at 918.6 eV (labelled with A in Table SI 1) was assigned to the ^1G multiplet of the two-localized-hole d^8 final state [23, 25], which splits in various multiplet states corresponding to structures seen in Figure SI 1b (Electronic supplementary material). The peaks assigned to the ^3P and ^1D final state transitions were not resolved and contributed to one signal at 919.8 (0.1) eV (peak labelled with D in Table SI 1) in agreement with literature [24, 26, 27]. An additional peak detected at 916.5 (0.1) eV could not be explained on the basis of theoretical calculations carried out on the structure of the copper Auger multiplet signals but according to some authors might be assigned to the

presence of satellites [28, 29]. Their origin is still debated but this topic is behind the scope of this investigation. Parameters used for the curve fitting of this signal are provided in Table SI 1. Earlier, curve fitting of x-ray induced Auger signals was based on empirical approach [12 – 14].

Zinc: The $Zn2p_{3/2}$ signal acquired on sputtered zinc (Figure SI 2a) showed a single peak at 1021.6 (0.1) eV, the fit parameters are listed in Table SI 2. Similarly to copper also the $ZnL_3M_{45}M_{45}$ Auger signal (Figure SI 2b) exhibited a complex fine structure and the signals related to ^1S, ^3P, ^1D, ^3F and ^1G final states were identified. The most intense peak was ascribed to ^1G final state transition (KE 992.1 (0.1 eV)), which is the most probable transition [24]. The peaks assigned to the ^3P and ^1D final state transitions are not resolved and they form one signal at 993.5 (0.1) eV. In agreement with the literature [24, 26] between the ^1G and ^1S signals an additional peak (989.6 (0.1) eV) is present that could not be explained on the basis of theoretical calculations carried out on the structure of the zinc Auger multiplet signals and also in this case might be tentatively assigned to the satellite structure [28]. Parameters used for the curve fitting of the spectra are provided in Table SI 2.

3.1.2.Copper and zinc oxides

CuO, Cu_2O and ZnO were analysed as reference materials by XPS using the same analysis conditions applied for the acquisition of the data on the model brass alloy. In this way was possible obtaining the curve fit parameters of the photoelectron and of the XAES signals.

Copper oxide CuO: The survey spectra of CuO (not shown) showed all the characteristic signals of copper and oxygen. C1s peak was observed due to an adventitious contamination from air exposure. The most intense photoelectron peak of copper, $Cu2p_{3/2,}$ was found at a BE of 933.8 (0.1) eV (Figure SI 3a) and it was accompanied by two strong satellites at the high BE side of the main peak, due to a d^9 characteristic configuration of compounds containing Cu(II) ($3d^9$) [23, 28, 29]. The differences between the BE of the satellites and of the main peak were found to be + 7.7 (0.1) eV as also reported by other authors [5, 13]. The curve fitting parameters of $Cu2p_{3/2}$ are listed in Table SI 3.

The $CuL_3M_{4,5}M_{4,5}$ Auger signal (Figure SI 3b) is quite different from those of the pure copper (Fig. SI1b) due to the difference in the ground state, d^9 for Cu(II) and d^{10} for Cu(0) and to the presence of

the oxygen in the structure. It was found to be multicomponent and the kinetic energy (KE) of most intense peak (^{1}G, labelled with A in Table SI 3) was 917.8 (0.1). The KE values of all the components and the curve fitting parameters of the Auger signal of CuO are presented in Table SI3. The O1s high-resolution signal is provided in Figure SI 3c. The O1s signal of the copper (II) oxide appears at 530.1 (0.1) eV; an additional signal was observed at 531.7 (0.1) eV due to the presence of hydroxide on the surface of the powder according to Chawla et al. [30]. In Table SI 3 peak energy and fit parameters for oxygen are listed.

Copper oxide Cu_2O: Besides the photoelectron and the Auger lines due to copper, also the signals attributable to oxygen and carbon were detected in the survey spectra of Cu_2O. The carbon signal is likely due to the ambient exposure during the sample preparation and transfer into the spectrometer. The maximum of the $Cu2p_{3/2}$ high-resolution spectrum (Figure SI 4a) was found at 932.4 (0.1) eV in agreement with [13]; curve-fitting parameters are provided in Table SI 4. Unlike CuO, the $Cu2p_{3/2}$ spectrum of Cu_2O did not show a satellite structure and the FWHM of the peak height is much lower than that of the signal of CuO. The $CuL_3M_{4,5}M_{4,5}$ Auger spectra (Figure SI 4b) exhibited a complex shape as a result of different final states. The KE values and the parameters used for the curve fitting of Cu_2O Auger signal are presented in Table SI 4. The curve fitting was performed using four components in agreement with [12 – 14] while for metallic copper five components were used. The main peak related to the ^{1}G final state transition, which is the most probable transition, showed a KE of 916.8 (0.1) eV. The O1s signal (Figure SI 4c) was located at ca. 530 eV (Table SI 4C). The fit resulted to be the convolution of three components: the most intense one at 530.3 (0.1) eV due to the copper (I) oxide and the other two components which might be related to the presence of a thin organic contamination layer and to adsorbed water in the outer part of the sample surface.

Zinc oxide ZnO: The $Zn2p_{3/2}$ signal (Figure SI 5a) was found at 1021.6 (0.1) eV, curve-fitting parameters are given in Table SI 5. The $ZnL_3M_{45}M_{45}$ Auger peak (Figure SI 5b) showed a general broadening and the satellite structure at low KE was less pronounced than in the metallic state, in agreement with [9, 11]. The KE values and curve-fitting parameters for the individual signals are given in Table SI 5. The oxygen O1s signal of ZnO (Figure SI 5c) showed three peaks, the curve-fitting

parameters are given in Table SI 5.

The main result of this section on copper and zinc reference compounds is the theory based curve-fitting of the XAES signals of both metallic (Figure SI 1b, SI 2b) and oxide compounds (Figure SI 3b, SI 4b) of copper and zinc. Differences in kinetic energies and area ratios of the individual XAES signals were maintained constant, so *XAES envelopes* characterized by the KE and the intensity of the main peak could then be used in curve fitting of more complex systems such as brass alloys.

3.2. Brass model alloy Cu37Zn

3.2.1. Brass Cu37Zn model alloy "as received"

The model alloy, brass Cu37Zn, was first characterized in the "as received" state. The survey spectra (Figure SI 6) revealed the presence of the elements constituting the alloy, the oxygen signal and a very intense peak of carbon located at 285.0 eV. The carbon 1s signal showed three components: the main component at 285.0 eV (aliphatic carbon), a second component at 286.6 (0.1) eV due to –COH or -COC bonds and a third component at higher BE (289.1 (0.1) eV) that could be assigned to carbon atoms in COO functional groups or to carbonates.

The high-resolution spectra of $Cu2p_{3/2}$, $Zn2p_{3/2}$, $CuL_3M_{4,5}M_{4,5}$, $ZnL_3M_{4,5}M_{4,5}$ and O1s are shown in Figure 1; the energy values and the fit parameters are listed in Table 1. The $Cu2p_{3/2}$ spectrum (Figure 1a) showed the characteristic shake-up satellites of a Cu^{2+} compound. The BE of 934.9 (0.1) eV is 1.0 eV higher compared to CuO (Table SI3). The reason might be ascribed to the presence of copper (II) hydroxide in agreement with other authors [11, 13, 30, 31]. The $Zn2p_{3/2}$ signal at 1022.4 (0.1) eV is 0.8 eV more positive compared to the pure ZnO (Table SI 5); this might be due to the presence of zinc hydroxide as reported by [1, 2].

The Auger spectra of both copper $CuL_3M_{4,5}M_{4,5}$ (Fig. 1b) and zinc $ZnL_3M_{45}M_{45}$ (Fig. 1d) showed five components. Those spectra differ from those of the oxides of copper (Fig. SI 3) and zinc (Fig. SI 4): the spectra are noisier and their components are broader (higher FWHM). The KE of the main peak

(A) of the copper CuLMM signal is shifted by 1.6 eV to lower values compared to CuO; the shift of ZnLMM with respect to ZnO is found to be -0.7 eV. Thus, approximately, the shift to more positive BE values of the 2p signals are equal to the shift to more negative kinetic energies of the Auger signals, resulting in the same Auger parameter (see discussion Section 4.3).

3.2.2. Brass Cu37Zn model alloy sputter cleaned

The Cu37Zn model alloy was also characterized after argon ion sputtering until complete disappearance of the contamination and the oxide layers (Figure SI7). Figure 2 shows the high-resolution spectra of the sputtered brass alloy: $Cu2p_{3/2}$, $Zn2p_{3/2}$, $CuL_3M_{45}M_{45}$, $ZnL_3M_{45}M_{45}$; Table 2 reports the electron energy values and the fit parameters of each signal. $Cu2p_{3/2}$ and $Zn2p_{3/2}$ show only one single peak at 932.7 (0.1) eV and 1021.3 (0.1) eV respectively.

The high-resolution spectra of copper (Fig. 2b) and zinc (Fig. 2d) Auger signals exhibited a complex fine structure similar to those of the metal ones (Figure SI 1b and SI 2b). Table 2 presents the electron energy values, and the fit parameters related to the acquired spectra.

3.2.2 Brass Cu37Zn model alloy mechanically polished

The model alloy Cu37Zn was analysed after mechanical polishing as described in Section 2.1. The survey spectra showed the characteristic signals of Cu, Zn, C and O (Figure SI 8). The high-resolution spectra of $Cu2p_{3/2}$, $Zn2p_{3/2}$, $CuL_3M_{45}M_{45}$, $ZnL_3M_{45}M_{45}$, O1s are shown in Figure 3. Energy values, FWHM and line shape (GL ratio and tail function) are provided in Table 3. The spectra line-shapes are different from those obtained on the pure compounds (see tables SI1-SI5) and these differences were attributed to the fact that on the alloy surface, after mechanical polishing, the contributions to the signal of both metal and oxide are simultaneously present. Furthermore, as it is apparent from the line-shapes reported in the SI, the curve fitting parameters are different for metals and oxides. Transition metals are characterized by exhibiting a tail at the higher binding energy side and the tail function takes into account electron-hole pair creation at the Fermi level for metallic systems [3].

$Cu2p_{3/2}$ and $Zn2p_{3/2}$ showed only one single peak with the same BE as in pure copper and zinc. The

XAES spectra of $CuL_3M_{45}M_{45}$ (Fig. 3b) and $ZnL_3M_{45}M_{45}$ (Fig. 3d) have a clearly different shape from those of pure metals and pure oxide compounds. In fact the copper and zinc Auger signals showed the simultaneous presence of the components assigned to the metal and to the oxides due to the presence of a thin oxide layer. The curve fitting of the $CuL_3M_{45}M_{45}$ and $ZnL_3M_{45}M_{45}$ Auger peaks of copper and zinc was performed using the envelopes of the metallic states (shown in Fig. SI 1b and SI 2b) and the oxidized ones (Figure SI 4c and SI 5c). This is to our knowledge the first time that Cu and Zn Auger signals of complex layered systems have been resolved in their components.

4. Discussion

XPS surface analysis usually relies on the most intense photoelectron signals. As it is well known, copper Cu 2p and zinc Zn 2p photoelectron signals do not exhibit a chemical shift between metallic and oxidized state. The BE values of metallic and oxidized zinc are reported at 1021.6 eV, and for metallic copper and Cu_2O the BE (932.5 eV in both cases) do not allow the univocal identification of the two states. Several papers [4, 6, 11 - 14] proposed thus the use of x-ray induced Auger signals (XAES) where clear shifts in KE and changes in the shape of the spectra are found between metals and oxides. Regarding the quantitative analysis of copper-zinc alloys (brasses) with an oxidized surface layer in the nano-meter range literature only reports few examples[11-14]. In the following a novel approach for univocal assignment to the various copper and zinc chemical states when they are simultaneously present is described together with the description of a quantitative analysis method to be followed when a thin-layer of copper and zinc oxy-hydroxides is present on the surface of the alloy.

4.1. Curve fitting of x-ray induced Auger spectra

The XAES signals of pure copper and zinc metals and oxides are composed of several peaks that were here assigned following the results of the theoretical approach reported in literature predicting the differences in KE and intensity ratio (Table SI 1, SI 2, SI 3, SI 4 and SI 5) [7, 9, 23, 26, 29]. In this work the

spectra of metallic copper and zinc (Fig. SI 1b, SI 2b) as well as copper and zinc oxide reference compounds (Fig. SI 3c, SI 4c, SI 5c) have been measured and processed. Each spectrum (envelope) could be reproduced based on the individual components and then used for the subsequent curve fitting of complex signals. A similar but empirically based approach for curve fitting of x-ray induced Auger signals of copper and zinc was proposed by other authors but the best results were reported by [12–14] where reference spectra of various compounds were characterized under controlled conditions.

XAES for the sputtered Cu37Zn alloy compared to metallic copper and zinc: the XAES signal for metallic copper (Figure SI 1c) agrees well with the signal of copper in the sputtered brass alloy (Fig. 2b) as qualitatively reported also in literature [11]. The KE of the main peak (A) assigned to ^{1}G is found at 918.6 eV for metallic copper and for copper in the alloy. In addition, the energy difference between the individual signals and the intensity ratio are perfectly identical (compare Table SI 1 with Table 2). Also the signals of pure zinc (Fig. SI 2b) and zinc in the brass alloy (Fig. 2d) are similar. A slight shift of the KE of the main peak (A) assigned to ^{1}G of + 0.2 eV is found (compare Table SI2 with Table 2). The energy difference and the intensity ratios between the individual signals are reasonably identical for pure zinc (Table SI 2) and zinc in the sputtered alloy (Table 2).

Regarding the binding energies, BE of copper $Cu2p_{3/2}$ is shifted by + 0.2 eV in the alloy and BE of zinc $Zn2p_{3/2}$ by -0.3 eV. The same results were found in studies of Cu-Zn alloys [11, 32]. These small differences can be attributed to changes in the electronic environment going from the pure metal to the alloy. The lattice parameter of the cubic face centred lattice increases from 3.608 Å for pure copper to 3.696 Å for alloys containing 37% of zinc. Hence, the electron distribution on each atom can be expected different for pure copper and for the Cu37Zn alloy. Positive shifts for the BE and (nearly equal) negative shifts for the KE result in the same Auger parameter α', thus in similar final state effects.

XAES for the "as received" Cu37Zn alloy compared to copper and zinc oxides: a comparison of the XAES signal of ZnO (Fig. SI 5b) and the ZnLMM signal of the "as received" Cu37Zn alloy shows good agreement. In particular, the difference between the kinetic energies of the individual signals and

their intensity ratios is identical in pure ZnO (Table SI5) and in the "as received" alloy (Table 1). A shift of – 0.7 eV is found for the KE of the ZnLMM signal in the alloy (compare to the shift of + 0.8 eV in the $Zn2p_{3/2}$ signal).

A comparison of the XAES signals for copper oxide Cu_2O (Fig. SI 4c), CuO (Fig. SI 3b) and the copper oxi-hydroxides of the "as received" brass alloy (Fig. 1b) showed clear differences, thus at the surface of the "as received" alloy a different copper-compound is likely to be present. Based both on the $Cu2p_{3/2}$ (Fig. 1a) and the Cu LMM signal (Fig. 1b) the presence of mainly copper hydroxide in the outer part of the surface film can be envisaged in agreement with what already reported in [13]. Using the chemical state plot (Section 4.3) the species present at the surface of the as received alloy will be identified.

4.2. Quantitative analysis

Quantitative analysis in a system such as brass alloy with a thin oxidized surface film is not possible because the copper and zinc 2p signals do not distinguish between metallic and oxidized states. Only the x-ray excited Auger signals allow a clear and quantitative distinction between metallic and oxidized state (Fig. 3b, 3d). Here a procedure and a formula that allows transfer the experimental intensity ratio from the LMM to the (unknown) intensity ratio of the 2p signals is presented.

4.2.1. Ratio between 2p photoelectron and LMM x-ray excited Auger electron signals

In the case of copper and zinc reference compounds as well as for the Cu37Zn brass alloy after sputtering and in the as received state, both the x-ray excited Auger signals and the 2p photoelectron signals are due to only one chemical state, either metallic or oxidized. Thus on these samples the experimental intensity ratio, R, defined as: $R = I_{2p} / I_{LMM,}$ could be determined. Peak areas I_{2p} and I_{LMM} obtained following the curve fitting of the spectra were corrected for transmission function Q(E) [20] and attenuation lengths Λ [21].

The experimentally determined intensity ratio R (Table 4) is, as expected, different for copper and zinc, but it also results different for the metallic (R_{met}) and the oxidized (R_{ox}) state. Thus, the common assumption of an element specific sensitivity factor S or cross section σ for a given transition independent on its chemical environment cannot be here applied. In addition the values of R depend on the geometry of the instrument (Table 4). In order to calculate the surface composition independently on the spectrometer geometry, it is here proposed a correction factor k, defined as $k = R_{ox}/R_{met}$ (Table 4, shadowed area). Indeed, the correction factors k are independent on the instrument and k = 1.5 for copper and k = 0.8 for zinc have been found (Table 4).

The experimentally determined ratios R between the photoelectron intensity I_{2p} and the Auger signal intensity I_{LMM} for the "as received" Cu37Zn alloy were found to be very different from CuO (Table 4). This is due to the different attenuation of the photoelectrons (ca. KE = 552 eV) and of the x-ray excited Auger electrons (ca. KE = 917 eV) by the thick contamination layer on the as-received alloy. Assuming 5 nm contamination (Table 8), the attenuation of the 2p photoelectrons is twice as strong as for the x-ray excited Auger. The attenuation corrected ratio R is within the range of the pure oxide and, as a consequence, also the k value is identical (Table 4). The same reasoning holds for the zinc signals.

For brass alloys with a thin surface film (as example the mechanically polished sample, Fig. 3) the CuLMM (Fig. 3b) and ZnLMM (Fig. 3d) spectra allow determining the intensity of the metallic and the oxide contribution. From these intensities the intensity ratio $r = LMM_{ox}/LMM_{met}$ is calculated. For copper this was found r equal to 1 while for zinc it was found equal to 4 (Table 5). The experimentally determined intensity ratio in the x-ray induced Auger signals, r, and the correction factor k (from Table 4) allow calculate the corresponding intensity ratio for the 2p signals. The equation derived (appendix A) for the calculation is:

$$\%2p_{ox} = \frac{100 \cdot r \cdot k}{(1 + k \cdot r)} \qquad \text{eq. (2)}$$

k is the (element specific) correction factor (Table 4)

r is the experimentally determined ratio of the x-ray induced Auger signals of the same element but in different oxidation state: LMM_{ox}/LMM_{met} (Table 5)

The calculated percentage of oxidized and metallic compound in the 2p signal is shown in Figure 4 for both copper and zinc as a function of the input data $r = LMM_{ox}/LMM_{met}$.

Table 5 reports the input parameters and the corresponding calculated results. It can be noted that for copper the intensity of the oxide increases by ca. 20% (from 50 to 60%) whereas for zinc the intensity of the metal increases by 20% (from 20 to 24%).

The theoretical background of this empirical approach, especially of the intensity ratio $R = I_{2p} / I_{LMM}$ (Table 4) can be discussed. While the intensity ratios of different x-ray excited Auger signals, e.g. $L_{23}M_{45}M_{45}$ / $L_{23}M_{45}M_{45}$ for Ni, Cu and Zn could be related to the effective charge Δq on the metal atom in the different compounds [32], such a theoretical basis for the intensity ratio between 2p photoelectron and LMM x-ray excited Auger electrons signals is lacking. An attempt to use intensity ratio between 2p photoelectrons and LMM Auger electrons was made to quantify Cu_2O on Cu [12]. In later studies [13, 14] the ratio of experimental intensities I_{2p}/I_{LMM} was used to determine the sensitivity factor for the Auger signals σ_{LMM} of copper and zinc, assuming this factor to be the same for metallic and oxidized compounds. As in this work R_{ox} and R_{met} are different both for copper and zinc (see Table 4) meaning that also the calculated cross sections $\sigma_{LMM,ox}$ and $\sigma_{LMM,met}$ are different. The assumption of equal cross section [12 – 14] does not hold for complex layered systems.

Only the experimentally determined factor $k = R_{ox}/R_{met}$ as proposed in this work, is characteristic for an element (copper, zinc), reasonably constant and independent on the instrument used for the analysis. Thus the factor k can be used to convert ratios LMM_{ox}/LMM_{met} resulted from the curve fitting of x-ray excited Auger signals (Fig. 3b, 3d) to intensity ratios of the photoelectron signal $2p_{ox}/2p_{met}$ needed for obtaining the intensities of each metallic and oxidized component. These data are required for the quantitative analysis of nano-structured layered systems (see Section 4.2.3.).

4.2.2. Quantitative analysis of Cu37Zn model brass alloy

Sputtered Cu37Zn model brass alloy: After slight Ar^+ sputtering no oxides were detected on the surface of the alloy here examined: both Cu2p and Zn2p photoelectron signals and corresponding XAES signals (Figure 2) refer to the metallic state only. Quantitative analyses were performed following the first principle model and the results are summarized in Table 6. The difference with the nominal composition can be ascribed to a preferential sputtering effect that was already reported in [34].

Cu37Zn model alloy "as received": in the as received state, even after a very slight sputtering to only remove the contamination layer, no signals from the underlying alloy were detected. Thus both the Cu and Zn 2p photoelectron signals and the XAES signals (Figure 1) refer to the oxidized state only. Quantitative analysis has been performed following the first principle approach. The results are presented in Table 7.

4.2.3. Quantitative surface analysis of brass alloys with thin oxide film

Mechanically polished Cu37Zn model brass alloy: The XAES spectra of both copper (Fig. 3b) and zinc (Fig. 3d) show the presence of metallic and oxidized components, indicating a thin oxide layer on the brass surface. XAES areas were used to calculate the ratio r of metallic and oxidized copper and zinc respectively (Table 5). The intensities of the metallic and oxidized components in the 2p photoelectron signal were calculated following the approach outlined above in 4.2.1, results of one example are provided in Table 5.

Once the photoelectron intensities $I_{Cu,met}$, $I_{Cu,ox}$, $I_{Zn,met}$ and $I_{Zn,ox}$ and of the contamination I_c are known (Table 5), the quantitative analysis of such a thin-layered system was performed following the three-layer model [22,35,36], assuming the presence of a contamination layer and of a homogeneous oxide film on top of the alloy. The density for Cu37Zn alloy was taken as 8.5 g/cm^3, the density of the oxide film was assumed to be 6 g/cm^3 (6.14 g/cm^3 for Cu_2O and 5.61 g/cm^3 for ZnO). The results of the

quantitative analysis of the mechanically polished Cu37Zn alloy obtained for three different analysis points are illustrated in Table 8.

They are consistent: a thin oxide film is present on the surface of the alloy. The oxide film is rich in copper oxide (Cu_2O) and contains about 33% of zinc oxide (ZnO). The alloy composition beneath the oxide film is in average very close to the nominal composition, 64.5 (1.5) % copper and 35.5 (1.5)% zinc. One of three samples even shows 37% zinc.

4.3. Chemical state plot

The chemical state identification using XPS surface analysis has became routine for most of the elements in the periodic Table [4]. However, for copper and zinc the chemical state identification based on the BE only is challenging since it is not possible distinguish between Zn (II) and Zn (0) in the Zn2p and between Cu (I) and Cu (0) in the Cu2p spectra [4]. While the photoelectron signals of copper and zinc showed the same BE, the Auger signals of both elements are different from their pure elements (Figure SI1 – SI4). Moretti [11] has shown that the chemical state plot and the modified Auger parameter concept are particularly important for copper and zinc compounds because the two dimensional representation of photoelectron BE versus XAES KE, Wagner chemical state plot, allows a more accurate assignment. Other examples of successful application are sulphur compounds in sulphur containing minerals [8], the chemical state of phosphorus in amorphous alloys [37], phosphate glasses [38] or in nickel-phosphorus coatings [39].

Copper compounds: Wagner chemical state plot of copper is shown in Figure 5; KE, BE and Auger parameter of the different compounds are summarized in Table 9. The reference compounds (metallic copper, CuO, Cu_2O and in addition $Cu(OH)_2$) [13] are shown together with copper in the Cu37Zn model brass alloy after Ar^+ ion sputtering, after mechanical polishing and in the "as received" state. Metallic copper and Cu_2O have the same BE at 932.5 (0.1) eV whereas CuO and $Cu(OH)_2$ clearly show higher

binding energies. Interesting to note that the Auger parameter (Table 9 and diagonal line in the plot) α' = 1851.0 (0.2) eV is the same for metallic copper and $Cu(OH)_2$, indicating a similarity of the copper chemical state. Cu_2O instead, a copper Cu(I) compound, has an Auger parameter of α' = 1849.2 (0.2) eV (Table 9).

The copper signal of the sputtered alloy Cu37Zn coincides with that of the metallic copper. Copper in the "as received" alloy is found close to the $Cu(OH)_2$ standard, confirming that the outmost surface is mainly of copper hydroxide. The mechanically polished alloy showed two points: one that coincides with metallic copper, the other with Cu_2O. This indicates that on top of the alloy a thin oxide film is present (see Section 4.2.3). If, as very often is done, only the most intense Auger line of copper (918.5 (0.1) eV, Figure 3b) were used for speciation, the presence of Cu_2O would not have been revealed.

Zinc compounds: Wagner chemical state plot of zinc is shown in Figure 6; KE, BE and modified Auger parameter of the different compounds are summarized in Table 9. Zn(II) and Zn(0) compounds cannot distinguished on the basis of the BE. Considering also the x-ray excited Auger signals and the chemical state plot, different chemical states became distinguishable. The Auger parameter (Table 9) for metallic zinc is α' = 2013.7 (0.2) eV, for ZnO and $Zn(OH)_2$ (both Zn(II) compounds) the Auger parameter is α' = 2009.7 $\pm$ 0.2 eV. This is mainly due to a difference in the XAES Zn LMM kinetic energy (Table 9). Wagner plot shows that at the surface of the mechanically polished sample both metallic zinc and ZnO could be detected, thus supporting that a thin oxide layer is present on top of the alloy. As mentioned above for copper, if only the most intense Auger line of zinc (988.0 (0.1) eV, Figure 3d) would have been considered only the presence of ZnO but not of metallic zinc would have been revealed.

5. Conclusions

The following conclusions can be drawn from this surface analytical work:

1. A new analytical strategy for simultaneous chemical state identification and quantification of

copper and zinc in complex, thin-layered systems has been established.

2. Curve fitting of the multicomponent X-ray excited Auger spectra of copper $CuL_3M_{4,5}M_{4,5}$ and zinc $ZnL_3M_{4,5}M_{4,5}$ allows the discrimination of the different chemical states (e.g. metallic and oxide components) in complex systems
3. The kinetic energies of the curve fitted Auger signals allow an unambiguous assignment of the chemical state of copper and zinc compounds with the chemical state plot
4. Standards of pure metals and oxides are essential to accurately determine the envelopes of the complex Auger signals for curve fitting and to calculate the experimental intensity ratios $R = I_{2p} / I_{LMM}$ between photoelectron and Auger intensity required for quantification
5. The experimentally determined quantification factor $k = R_{ox}/R_{met}$ as proposed in this work is characteristic for an element (copper, zinc), reasonably constant and independent on the instrument used for the analysis.
6. The composition of the alloy beneath the thin oxide film of mechanically polished samples of Cu37Zn calculated with the new analytical strategy presented in this paper is found to be very close to the nominal composition.
7. The new analytical approach for quantification has been tested on Cu37Zn model brass alloys after different surface pre-treatments and has proven to be successful.

Acknowledgments

The Italian Ministry of University and Research (MIUR) is thanked for financing the PRIN project prot. 2010329WPF_005 "Sustainability in cultural heritage: from diagnosis to the development of innovative systems for consolidation, cleaning and protection".

The authors wish to express their gratitude to Istituto Nazionale di Previdenza Sociale (National Social Security Institution), for its support of this work.

Sardinia Regional Government is gratefully acknowledged for the financial support (P.O.R. Sardegna F.S.E. Operational Program of the Regione Autonoma della Sardegna, European Social Fund 2007 – 2013 – Axis IV Human Resources, Objective 1.3, Line of Activity 1.3.1 "Avviso di chiamata per il finanziamento di Assegni di Ricerca").

The authors wish to express their gratitude to Prof. Nicholas D. Spencer (Laboratory for Surface Science and Technology ETH Zürich, Switzerland) for the access to the Quantera. Mr. Cossu is acknowledged for the technical maintenance of the spectrometers.

References

1. NIST Standard Reference Database 20 Version 4.1, http://srdata.nist.gov/xps, (accessed November 2015)
2. J.F. Moulder, W.F. Stickle, P.E. Sobol and K.D. Bomben, Handbook of X-ray Photoelectron Spectroscopy, Perkin-Elmer Corp., Physical electronics, Minnesota, 1992
3. D. Briggs and J.T. Grant, Surface Analysis by Auger and X-ray Photoelectron Spectroscopy, IM Publications and Surface Publication Data, West Sussex, 2003
4. M.C. Biesinger, L.W.M. Lau, A.R. Gerson and R.S.C. Smart, *Applied Surface Science*, 2010, ***257*****,** 887-898.
5. D.C. Frost, A. Ishitani and C.A. McDowell, *Molecular Physics*, 1972, **24**, 861-877.
6 P.E Larson, *Journal of Electron Spectroscopy and Related Phenomena,* 1974, **4**, 213-218.
7 I. Platzman, R. Brener, H. Haick and R. Tannenbaum, *Journal of Physical Chemistry C*, 2008, **112**, 1101-1108
8 M. Fantauzzi, D. Atzei, B. Elsener, P. Lattanzi and A. Rossi, *Surface and Interface Analysis*, 2006, **38**, 922-930.
9 G. Deroubaix and P. Marcus, *Surface and Interface Analysis*, 1992, **18**, 39-46
10. E. Antonides and G.A. Sawatzky, *Journal of Physics C-Solid State Physics,* 1976, **9**, 547-552
11. G. Moretti, *Journal of Electron Spectroscopy and Related Phenomena,* 1998, **95**, 95-144
12. H.D. Speckmann, S. Haupt and H.H. Strehblow, *Surface and Interface Analysis*, 1988, **11**, 148-155
13. P. Druska and H.H. Strehblow, *Surface and Interface Analysis*, 1995, **23**, 440-450
14. I. Milosev and H.H. Strehblow, *Journal of the Electrochemical Society*, 2003, **150**, 517-524
15. B. Elsener, M. Alter, T. Lombardo, M. Ledergerber, M. Wörle, F. Cocco, S. Palomba, M. Fantauzzi, A. Rossi, *Microchemical Journal*, doi: 10.1016/j.microc.2015.10.027 in press
16. N. Fairley, CASAXPS (Version 2.3.15), Casa Software Ltd, Wilmslow, UK, 2010
17. D.A. Shirley, *Physical Review B*, 1972, **5**, 4709-4714
18. J.H. Scofield, *Journal of Electron Spectroscopy and Related Phenomena,* 1976, **8**, 129-137
19. R.F. Reilman, A. Msezane and S.T. Manson, *Journal of Electron Spectroscopy and Related Phenomena,* 1976, **8**, 389-394
20. M. Fantauzzi, A. Pacella, J. Fournier, A. Gianfagna, G.B. Andreozzi and A. Rossi, *Analytical and Bioanalytical Chemistry,* 2012, **404**, 821-833
21. S. Tanuma, C.J. Powell and D.R. Penn, *Surface and Interface Analysis*, 2003, **35**, 268-275
22. A. Rossi and B. Elsener, *Surface and Interface Analysis*, 1992, **18**, 499-504
23. S.R. Barman and D.D. Sarma, *Journal of Physics-Condensed Matter*, 1992, **4**, 7607-7616

24. S.P. Kowalczyk, R.A. Pollak, F.R. McFeely, L. Ley and D.A. Shirley, Physical Review B, 1973, **8**, 2387-2391

25. J. Ghijsen, L.H. Tjeng, J. van Elp, H. Eskes, J. Westerink, G.A. Sawatzky and M.T. Czyzyk, *Physical Review B,* 1988, **38**, 11322-11330

26. E. Antonides, E.C. Janse, and G.A, Sawatzky, *Physical Review B*, 1977, **15**, 1669-1679

27. E.D. Roberts, P. Weightman and C.E. Johnson, *Journal of Physics C: Solid State*, 1975, **8**, L301-L304

28. G.G. Kleiman, *Journal of Electron Spectroscopy and Related Phenomena*, 1999, **100**, 17-34

29. G.G. Kleiman, R. Landers, P.A.P. Nascente and S.G.C. de Castro, *Physical Review B*, 1992, **46**, 4405-4413

30. S.K. Chawla, N. Sankarraman and J. H. Payer, *Journal of Electron Spectroscopy and Related Phenomena*, 1992, **61**, 1-18

31. N.S. McIntyre and M.G. Cook, *Analytical Chemistry*, 1975, **47**, 2208-2213

32. J.A. Rodriguez and J. Hrbek, *Journal of Vacuum Science and Technology*, 1993**, 11**, 1998-2002

33. S. Yashonath and M.S. Hedge, *Journal of Chemical Sciences, Proceedings Indian Academy of Sciences,* 1980, **89**, 489-494

34. G.E. Hammer and R.M. Shemenski, *Surface and Interface Analysis*, 1987, **10**, 355-359

35. D. De Filippo, A. Rossi, B. Elsener and S. Virtanen, *Surface and Interface Analysis*, 1990**, 15**, 668-674

36. A. Rossi and B. Elsener, *Materials Science Forum,* 1995, **185-188**, 337-346

37. B. Elsener and A. Rossi, *Electrochimica Acta,* 1992, **37**, 2269-2276

38. M. Crobu, A. Rossi, F. Mangolini and N.D. Spencer, *Analytical and Bioanalytical Chemistry,* 2012, **403**, 1415-1432

39. B. Elsener, D. Atzei, A. Krolikowski, V. Rossi Albertini, C. Sadun, R. Caminiti and A. Rossi, *Chemistry of Materials,* 2004, **16**, 4216-4225

Appendix A

Derivation of equation (2)

Definitions

R	experimentally determined intensity ratio 2p/LMM (see Table 4)
k	experimentally determined constant $k = R_{ox}/R_{met}$ (see Table 4)
r_{LMM}	experimentally determined intensity ratio in the Auger signal $r_{LMM} = I(LMM)_{ox}/ I(LMM)_{met}$
r_{2p}	unknown ratio in the 2p photoelectron signal $r_{2p} = I(2p)_{ox}/ I(2p)_{met}$

$r_{2p} = I(2p)_{ox}/ I(2p)_{met}$

$\%\ (2p)_{ox} = 100 * r_{2p} / (1 + r_{2p})$

$r_{2p} = k * r_{LMM}$

$\%\ (2p)_{ox} = 100 * k * r_{LMM} / (1 + k* r_{LMM})$ thus eq. (2) in the paper

Table 1: Binding energies and kinetic energies, FWHM of the peak height, line shape of O1s, $Cu2p_{3/2}$, $Zn2p_{3/2}$, $CuL_3M_{45}M_{45}$ and $ZnL_3M_{45}M_{45}$ of an as received Cu37Zn sample.

Peak	BE (eV ± 0.1)	FWHM (eV± 0.1)	Line shape
$Cu2p_{3/2}$	934.8	2.4	GL(70)T(1.5)
Sat 1	941.1	2.6	GL(30)
Sat 2	944.3	2.6	GL(30)
$Zn2p_{3/2}$	1022.4	2.1	GL(70)
O1s	530.7	1.7	GL(40)
O1s	532.0	1.7	GL(40)
O1s	533.3	1.7	GL(40)

Signal	KE (eV ± 0.1)	Assignment	Intensity ratio	FWHM (eV± 0.1)	Line shape
Cu LMM					
A	916.2	^1G	1	3.0	GL(30)
B	914.1		0.3	3.9	GL(30)
C	911.7	^1S	0.1	3.9	GL(30)
D	917.5	$^3P/^1D$	0.1	3.1	GL(30)
E	919.0	^3F	0.3	3.0	GL(30)
Zn LMM					
A	987.5	^1G	1	4.0	GL(30)
B	984.8		0.1	3.0	GL(30)
C	982.3	^1S	0.03	2.0	GL(30)
D	989.0	$^3P/^1D$	0.2	3.3	GL(30)
E	990.9	^3F	0.3	4.4	GL(30)

Table 2: Binding energies and kinetic energies, FWHM, line shape of $Cu2p_{3/2}$, $Zn2p_{3/2}$, $CuL_3M_{45}M_{45}$ and $ZnL_3M_{45}M_{45}$ of a sputtered Cu37Zn. Spectra were acquired using the Quantera^{SXM}.

Peak	BE (eV ± 0.1)	FWHM (eV± 0.1)	Line shape
$Cu2p_{3/2}$	932.7	0.9	GL(97)T(2)
$Zn2p_{3/2}$	1021.3	0.9	GL(92)T(1.5)

	KE (eV ± 0.1)	Assignment	Intensity ratio	FWHM (eV± 0.1)	Line shape
Cu LMM					
A	918.6	^1G	1	1.4	GL(80)
B	916.4	Sat.	0.3	1.9	GL(30)
C	914.1	^1S	0.3	2.2	GL(30)
D	920.0	$^3P/^1D$	0.1	1.0	GL(30)
E	921.4	^3F	0.3	1.4	GL(30)
Zn LMM					
A	992.3	^1G	1	1.7	GL(70)
B	989.5	Sat.	0.1	1.9	GL(70)
C	987.4	^1S	0.1	1.6	GL(70)
D	993.6	$^3P/^1D$	0.2	1.6	GL(70)
E	995.7	^3F	0.4	1.5	GL(70)

Table 3: Binding energies and kinetic energies, FWHM, line shape of C1s, O1s, $Cu2p_{3/2}$, $Zn2p_{3/2}$, $CuL_3M_{45}M_{45}$ and $ZnL_3M_{45}M_{45}$ of a Cu37Zn sample following mechanical polishing.

Peak	BE (eV ± 0.1)	FWHM (eV± 0.1)	Line shape
$Cu2p_{3/2}$	932.5	1.3	GL(70)
$Zn2p_{3/2}$	1021.7	1.7	GL (70)
O1s	530.4	1.6	GL (45)
O1s	531.8	1.6	GL (45)
O1s	533.3	1.6	GL (45)

Signal	KE (eV ± 0.1)	Attribution
CuLMM metal	918.5	envelope
Cu LMM oxide	916.8	envelope
Zn LMM metal	988.0	envelope
Zn LMM oxide	992.3	envelope

Table 4: Ratio of the 2p photoelectron and LMM x-ray excited Auger electron intensity and correction factor $k = R_{ox}/R_{met}$ for copper and zinc compounds: spectra were acquired with two spectrometers and areas were corrected for the geometry of the instruments.

System	Source	Intensity ratio R 2p/LMM		$k = R_{ox}/R_{met}$	
		Theta	Quantera	Theta	Quantera
Cu metal	**Pure metal**	3.4	2.0	1.56	1.5
Cu metal	**Sputtered alloy**	-	1.9	-	1.55
CuO	**Pure oxide**	5.3	3.0	1.56	1.5
Cu-oxide	**As rec. corrected**	5.1	3.0	1.5	1.5
Cu-oxide	**As received alloy**	2.5	1.5	0.74	0.75
Zn metal	**Pure metal**	3.8	2.3	0.79	0.74
Zn metal	**Sputtered alloy**	-	2.0	-	0.87
ZnO	**Pure oxide**	3.0	1.7	0.79	0.74
ZnO	**As rec. corrected**	3.2		0.83	
Zn-oxide	**As received alloy**	1.4	1.2	0.36	0.52

Table 5: Input parameters and results of calculations to determine the metallic and oxide intensity in the (unresolved) 2p photoelectron peak of copper and zinc (example of a mechanically polished sample)

Metal	% ox LMM	% met LMM	ratio r ox/met	correction factor k	% ox in 2p	I_{ox} 2p	I_{met} 2p
Copper	50	50	1	1.55	61	55066	35206
Zinc	80	20	4	0.8	76	41269	13068

Table 6: Composition of the sputtered Cu37Zn model brass alloy

Point	Contamination	Cu met	Zn met
1	nd	74%	26%
2	nd	80%	20%

Table 7: composition of the oxide film on the "as received" Cu37Zn model brass alloy

Point	Oxide film	Contamination	Cu ox	Zn ox
1	> 10 nm	4.5 nm	83	17
2	> 10 nm	3.8 nm	84	16
3	> 10 nm	4.5 nm	85	15
4	> 10 nm	4.0 nm	83	17

Table 8: Composition of the oxide film and the alloy beneath the oxide film formed on Cu37Zn model brass alloy after mechanical polishing. The thickness of the oxide layer and the contamination film are also given.

Area of analysis	Oxide film thickness (nm)	Contamination layer thickness (nm)	Cu ox wt%	Zn ox wt%	Cu met wt%	Zn met wt%
1	1.9	0.7	61	39	63.4	36.6
2	1.5	1.7	70	30	62.6	37.4
3	0.5	2.4	69	31	65.8	34.2

Table 9: BE and Auger KE of copper Cu $2p_{3/2}$, $Zn2p_{3/2}$, CuLMM and ZnLMM signals of the analysed compounds with the Auger parameters calculated using the different components for the Auger signals (α', column 3) and using only the most intense Auger line (α'_a, column 4).

	$BE_{photoelectron}$	KE_{Auger}	α'	α'
Copper				
Cu(0)	932.5	918.6	1851.1	1851.1
Cu_2O	932.4	916.8	1849.2	1849.2
CuO	933.9	917.8	1851.7	1851.7
Cu37Zn mech pol met	932.5	918.5	1851.0	1851.0
Cu37Zn mech pol ox	932.5	916.8	1849.3	-
Cu37Zn as received	935.0	916.2	1851.2	1851.2
Cu37Zn sputtered	932.7	918.6	1851.3	1851.3
Zinc				
Zn(0)	1021.6	992.1	2013.7	2013.7
ZnO	1021.3	988.1	2009.4	2009.4
Cu37Zn mech pol ox	1021.7	988.0	2009.7	2009.7
Cu37Zn mech pol met	1021.7	992.3	2014.1	-
Cu37Zn as received	1022.4	987.7	2010.1	2010.1
Cu37Zn sputtered	1021.7	992.3	2014.1	2014.1

Figure captions

Figure 1:
High-resolution spectra of Cu37Zn alloy “as received”.

Figure 2:
High-resolution spectra of the sputter-cleaned alloy Cu37Zn

Figure 3:
High-resolution spectra of the mechanically polished alloy Cu37Zn

Figure 4:
Percentage of oxidized component in the 2p signal versus percentage of the oxidized component in the LMM signal for copper and zinc

Figure 5:
Wagner chemical state plot of copper. The BE of $Cu2p_{3/2}$ and the KE of $CuL_3M_{4,5}M_{4,5}$ from this work after curve fitting taking into account the presence of the components due to oxidized copper are compared with the literature

Figure 6:
Wagner chemical state plot of zinc. The BE of $Zn2p_{3/2}$ and the KE of $ZnL_3M_{4,5}M_{4,5}$ from this work are compared with the literature

Figure 1

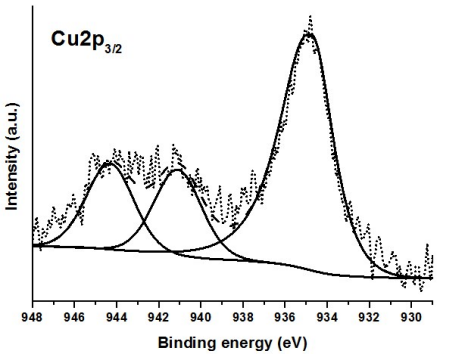

Figure 1a: $Cu2p_{3/2}$ peak

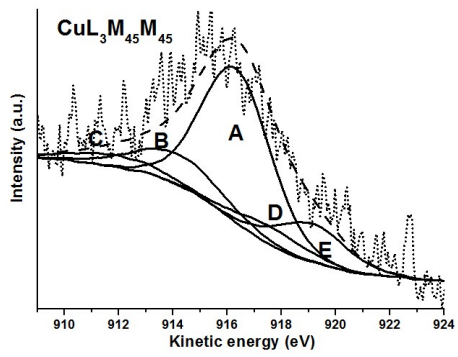

Figure 1b: $CuL_3M_{45}M_{45}$ peak

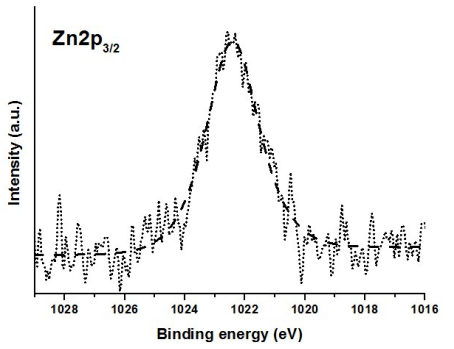

Figure 1c: Zn$2p_{3/2}$ peak

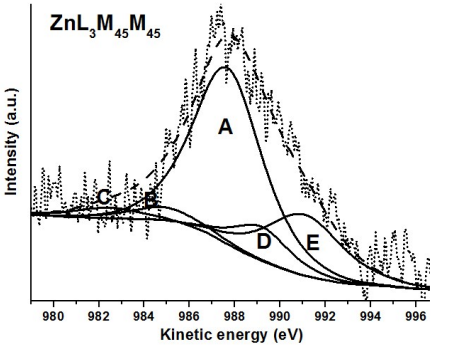

Figure 1d: $ZnL_3M_{45}M_{45}$ peak

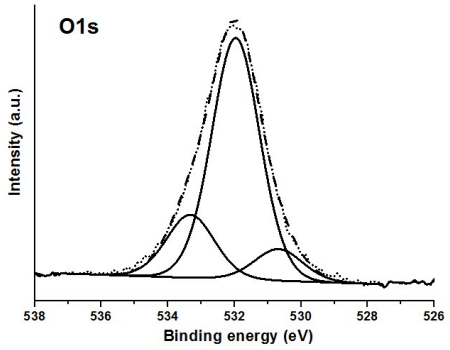

Figure 1e: O1s peak.

Figure 2

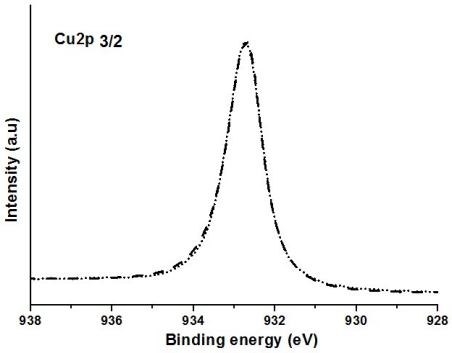

Figure 2a: $Cu2p_{3/2}$ peak

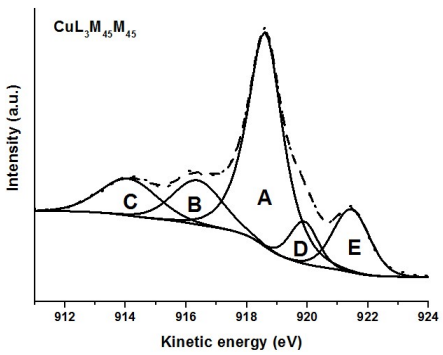

Figure 2b: $CuL_3M_{45}M_{45}$ peak

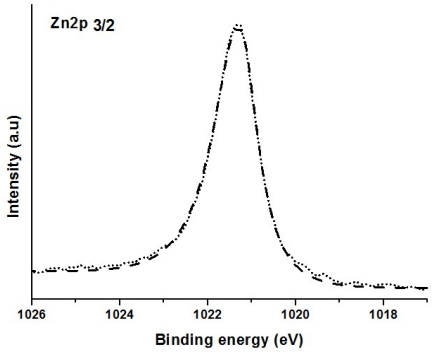

Figure 2c: **Zn**$2p_{3/2}$ peak

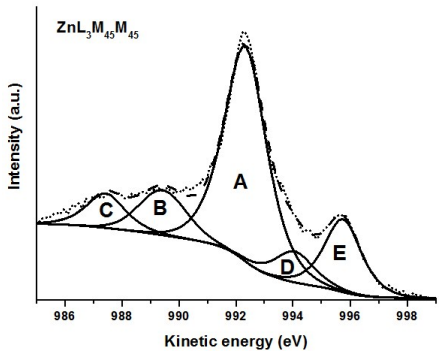

Figure 2d: $ZnL_3M_{45}M_{45}$ peak

Figure 3

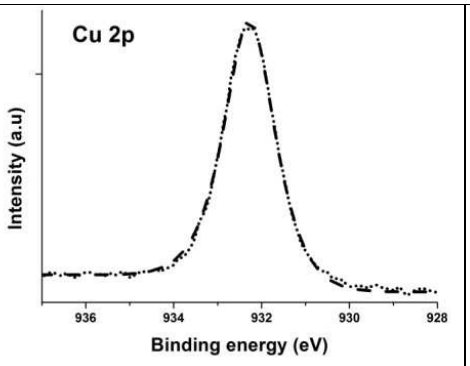

Figure 3a: $Cu2p_{3/2}$ peak

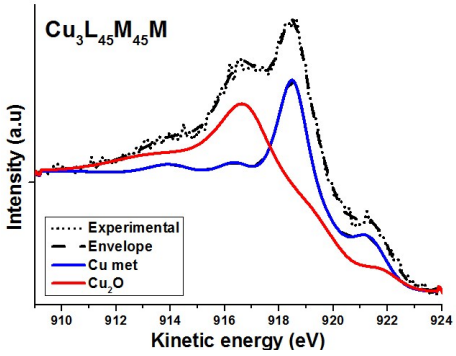

Figure 3b: $CuL_3M_{45}M_{45}$ peak

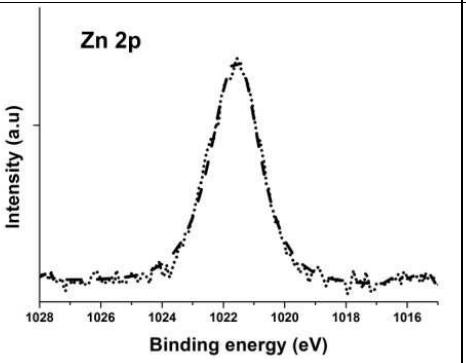

Figure 3c: $Zn2p_{3/2}$ peak

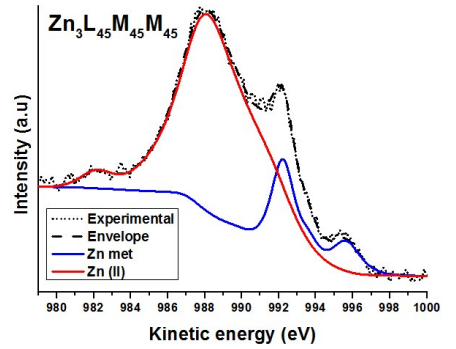

Figure 3d: $ZnL_3M_{45}M_{45}$ peak

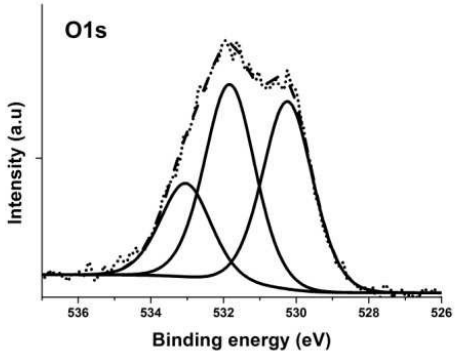

Figure 3e: O1s peak

Figure 4

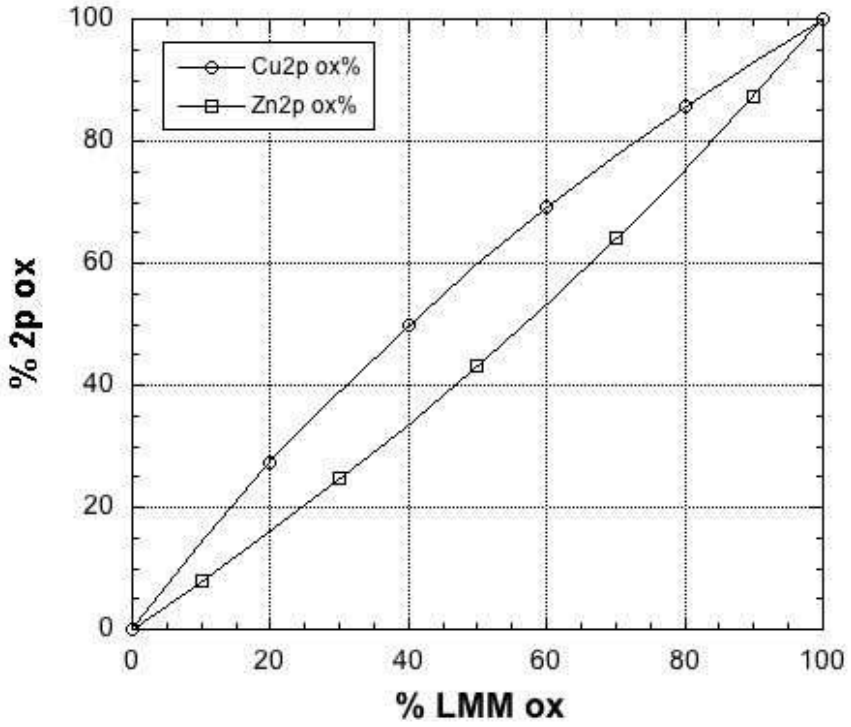

Figure 5

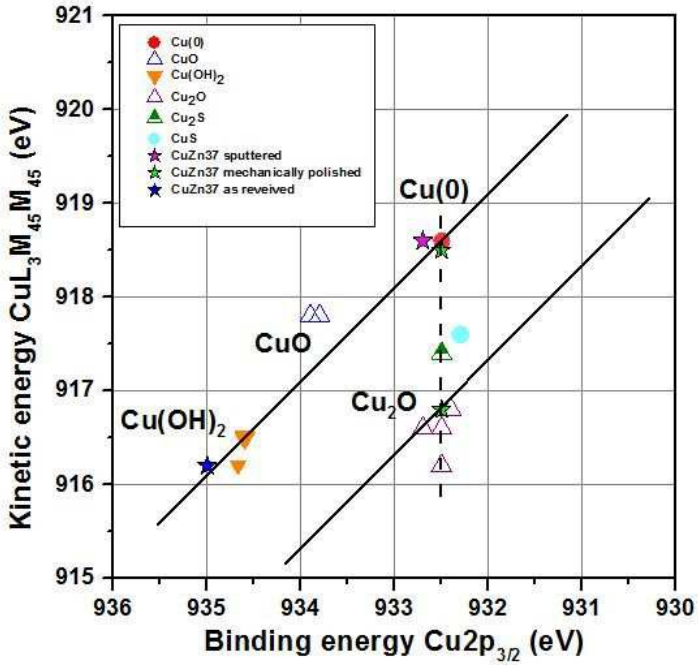

Figure 6

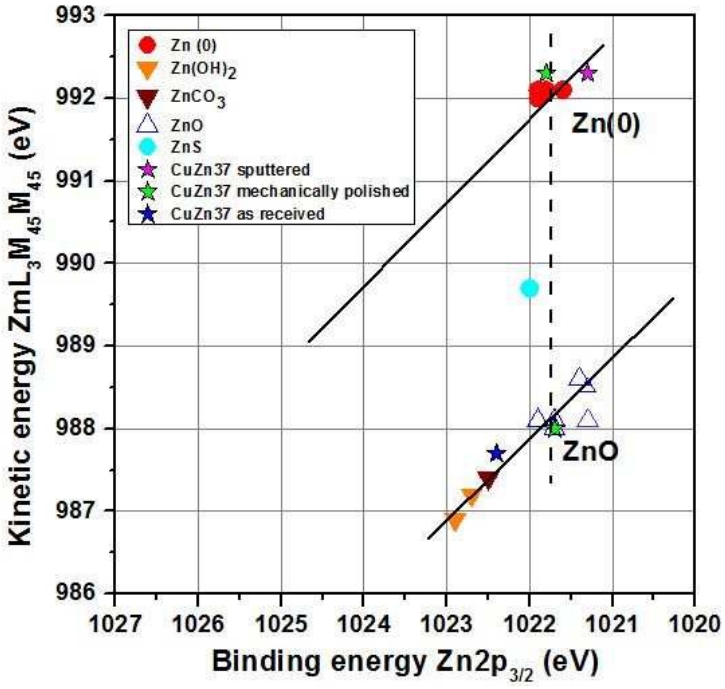

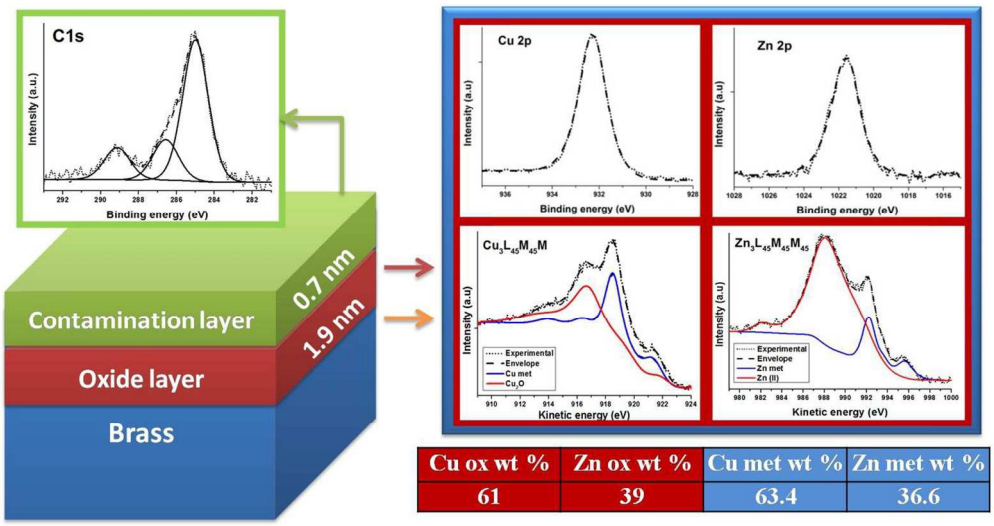

Cu ox wt %	Zn ox wt %	Cu met wt %	Zn met wt %
61	39	63.4	36.6

236x124mm (150 x 150 DPI)